Journal of Peptide Science
J. Peptide Sci. **10**: 363–380 (2004)
Published online 21 January 2004 in Wiley InterScience (www.interscience.wiley.com). DOI: 10.1002/psc.530

JOURNAL OF PEPTIDE SCIENCE

Conformational Study of Fragments of Envelope Proteins (gp120: 254–274 and gp41: 519–541) of HIV-1 by NMR and MD Simulations

MEENA KANYALKAR,[a] SUDHA SRIVASTAVA,[b] ANIL SARAN[a] and EVANS COUTINHO[a]*

[a] Department of Pharmaceutical Chemistry, Bombay College of Pharmacy, Kalina, Mumbai 400 098, India
[b] Tata Institute of Fundamental Research, Homi Bhabha Road, Colaba, Mumbai 400 005, India

Received 27 March 2003
Accepted 1 July 2003

Abstract: The envelope proteins, gp120 and gp41 of HIV-1, play a crucial role in receptor ($CD4^+$ lymphocytes) binding and membrane fusion. The fragment 254–274 of gp120 is conserved in all strains of HIV and, as a part of the full gp120 protein, behaves as 'immunosilent', but as an individual fragment it is 'immunoreactive'. When this fragment binds to its receptor, it activates the fusion domain of gp41 allowing viral entry into the host $CD4^+$ cells. The conformation of fragment 254–274 of the gp120 domain and fragment 519–541 of the gp41 domain was studied by NMR and MD simulations. The studies were carried out in three varied media — water, DMSO-d_6 and hexafluoroacetone (HFA). The fusogenic nature of the gp41 domain peptide was investigated by ^{31}P NMR experiments with model bilayers prepared from dimyristoyl-L-α-phosphatidylcholine (DMPC). The solvent was seen to exert a major effect on the structure of the two peptides. Fragment (254–274) of gp120 in DMSO-d_6 had a type I β-turn around the tetrad Val^9-Ser^{10}-Thr^{11}-Gln^{12} while in HFA a helical structure spanning the region Ile^5 to Gln^{12} was seen with the remaining part of the peptide in a random coil structure. It is possible that the β-turn may constitute an initiation site for the formation of the helix. In water at pH 4.5, the peptide adopted a β-sheet. The NMR results for fragment 519–541 of gp41 are conclusive of a β-sheet structure in DMSO-d_6, a conformation which may help in insertion into the membrane, a notion also put forward by others. The ^{31}P NMR studies of DMPC vesicles with this fragment show its fusogenic nature, promoting fusion of unilamellar vesicles to larger agglomerates like multilamellar ones.

Keywords: HIV-1; gp120; gp41; NMR; MD simulations; ^{31}P NMR; model membranes

INTRODUCTION

The acquired immunodeficiency syndrome (AIDS) is one of the most lethal diseases and is caused by human immunodeficiency virus (HIV) [1], a complex retrovirus encoding 15 distinct proteins. High-resolution electron microscopy has shown the HIV virion to have an icosahedral structure in which the viral envelope or the outer coat surrounds the inner core and is made up of a lipid bilayer. The outer layer glycoprotein called gp120 mediates receptor binding while gp41, the inner layer, mediates membrane fusion [2]. HIV's principal targets are the CD4 bearing helper T lymphocytes or T cells [$CD4^+$ ($T4^+$)] [3]. It is a protein found in the membrane of several types of immune system cells. It is now well established that direct interaction of HIV gp120 with a specific portion of the $CD4^+$ ($T4^+$) molecule is the most crucial point in inducing the infection [4, 5]. Gp120 is highly diverse both in size and sequence

*Correspondence to: Evans Coutinho, Department of Pharmaceutical Chemistry Bombay College of Pharmacy, Kalina, Mumbai 400 098, India; e-mail: evans-im@eth.net
Contract/grant sponsor: All India Council of Technical Education; Contract/grant number: 8017/RDII/MOD/DEG(38)/98–99.
Contract/grant sponsor: CSIR.

across the retrovirus family. Different functional roles have been described for each region of this molecule. The gp120 region has been subdivided into three domains that are separated by two conserved hinge regions. The amino terminal is the most variable region comprising V1 and V2 loops and an amphipathic helix (helix 1). The central region contains two helical regions helix 2 and helix 3 interspersed by a conserved turn known as the V3 loop. This region plays a significant role in cell tropism and post-binding events of fusion and infection. The carboxyl terminal region comprising V4 and V5 loops surrounds a fourth helical region. It comprises the principal region involved in binding to the cellular receptor.

There are reports [6] that suggest that an antiserum directed against fragment 254–274 of gp120, which belongs to the central conserved region, was efficient in neutralizing three different isolates of HIV *in vitro* but it did not block the binding of HIV to $CD4^+$ cells. Thus this well conserved region of gp120 appears to be involved in a post-binding event during virus penetration and represents an important target for antibody neutralization of HIV. It was also observed that this antisera immunoprecipitates a protein of 120 or 160 kD or both in HIV infected cells, while it did not immunoprecipitate in uninfected cells. This clearly indicates that the antisera only react with gp120. It was proposed that after the specific interaction of gp120 with $CD4^+$, the fragment 254–274 might undergo a suitable conformational change within the gp120–gp41 complex [7]. This structural alteration results in activation of the fusion domain (519–541) at the *N*-terminus of gp41 [8, 9] which can then mediate the fusion and thus allow virus penetration. This fusion peptide is essential for entry of the virus into the host $CD4^+$ T cell. On the other hand, the region 254–274 of gp120 may further bind to or interact with another $CD4^+$ molecule on the cell surface to facilitate HIV entry. All these events highlight the importance of fragment 254–274 of gp120 and fragment 519–541 of gp41 in the early events of the replicative cycle, i.e. when HIV binds to and enters the target cells [10].

There are also results that indicate that when fragment 254–274 is a part of gp120 it remains 'immunosilent'; however, by itself it is capable of efficiently neutralizing a number of HIV isolates. These findings suggest the potential of these particular regions of gp120 and gp41 in the development of a vaccine for AIDS. It also throws light on the fact that a small well-defined peptide may be a more effective vaccine that can specifically direct the immune response against a biologically important domain that is conserved in all strains of HIV. As a result, there is a great need to understand the structural aspects and structure–function relationship of these fragments of gp120 (254–274) and gp41 (519–541) that could be used to design small peptide vaccines for AIDS. Therefore the conformation of fragment 254–274: Cys^1-Thr-His-Gly-Ile^5-Arg-Pro-Val-Val-Ser^{10}-Thr-Gln-Leu-Leu-Leu^{15}-Asn-Gly-Ser-Leu-Ala-Glu^{21} in the gp120 domain (designated as P254) and fragment 519–541: Ala^1-Val-Gly-Ile-Gly^5-Ala-Leu-Phe-Leu-Gly^{10}-Phe-Leu-Gly-Ala-Ala^{15}-Gly-Ser-Thr-Met-Gly^{20}-Ala-Arg-Ser^{23} in the gp41segment (labelled as F519) were investigated. The conformation of these peptides was studied in three diverse media — water, DMSO-d_6 and hexafluoroacetone (HFA). In order to understand the fusogenic nature of F519 ^{31}P NMR experiments on the interaction of F519 with lipid bilayers were carried out.

METHODOLOGY

Materials and Sample Preparation

The conformation of P254 was investigated in DMSO-d_6, water at pH 4.5 and HFA (40% HFA + 5% D_2O + 55% H_2O) while F519 was studied in DMSO-d_6 and lipid bilayers prepared from dimyristoyl-L-α- phosphatidyl choline (DMPC). The conformation of F519 in water and trifluoroethanol (TFE) has already been reported [11]. The peptides (>97% purity) were purchased from Bachem (Switzerland), while the solvents DMSO-d_6 (99.9%), HFA and DMPC (99%) were purchased from Sigma Chemical Co. (USA). In DMSO-d_6 the concentration of P254 was 1.51 mM, while in water and HFA it was 2.26 mM. The concentration of F519 in DMSO-d_6 was 3.13 mM. At these concentrations, no aggregation was observed by NMR for either peptide.

NMR experiments were done on a Varian Unity Plus 600 MHz FT-NMR at 298 K. For resonance assignments, two dimensional (2D) Double Quantum Filtered COrrelated SpectroscopY (DQF-COSY) [12] and TOtal Correlated SpectroscopY (TOCSY) [13] were recorded. For deducing the conformation, 2D-Nuclear Overhauser Enhancement SpectroscopY (NOESY) [14] was recorded. For samples in water, solvent suppression was achieved

with the WATERGATE (water suppression by Gradient Tailored Excitation) technique for TOCSY and NOESY experiments [15, 16]. The number of transients was 32 for TOCSY and NOESY, and 64 for DQF-COSY. The mixing pulse (80 ms) in TOCSY was achieved by the MLEV-17 scheme. For all 2D-NMR experiments the fids were digitized with 2K points, except for DQF-COSY where it was digitized with 4K points. The number of experiments in the t_1 dimension was 512. Quadrature detection in the t_1 period was achieved by the hypercomplex (STATES) method. All 2D-NMR experiments were recorded with the conventional pulse sequences and a 1.5 s relaxation delay. The 2D data were processed using Felix software (v 97.0, MSI, USA) running on a Silicon Graphics O2 workstation. The fids were apodized by multiplication with a sine squared bell window function. In most of the experiments a $\pi/2$ phase-shifted sine squared bell window function was applied to the data along both dimensions. In some TOCSY and NOESY spectra, a $\pi/6$ sine squared bell window function was applied along D_1 axis and $\pi/3$ along D_2 axis, to obtain better resolution of overlapping peaks. The data were zero filled to give a final $2K \times 2K$ matrix except in the case of DQF-COSY, where a $4K \times 4K$ matrix was prepared prior to Fourier transformation.

The $^3J_{NH\alpha}$ coupling constants were extracted from the DQF-COSY spectrum, as follows. 1D slices were picked from the DQF-COSY spectrum and after a Hilbert transform the data was fast Fourier transformed. Zero filling was done to 64K points and a sine-squared window function shifted by 7° was applied to reduce the overlap. This trace was then complex Fourier transformed and the separation between antiphase components gave the coupling constants [17]. 1D spectra were recorded at different temperatures ranging from 298 K to 318 K. Over this temperature range, a linear dependence of the amide chemical shift on temperature was observed. Temperature coefficients of NH chemical shifts were calculated from TOCSY spectra recorded at 298 K, 303 K and 308 K. In aqueous solution, temperature coefficient values below 3 ppb/K indicate participation of the amide proton in intramolecular H-bonding. In HFA, the criterion for predicting intramolecular H-bonding differs from water. Temperature coefficients below 5 ppb/K suggest intramolecular H-bonds or solvent shielding in HFA [17]. ^{13}C chemical shifts were obtained from the Gradient enhanced Heteronuclear Single Quantum Coherence (HSQC) experiment [18]. ^{13}C chemical shifts helped to resolve any ambiguities in the assignment of spin systems, and were used to predict the secondary structure via the chemical shift index (CSI) [19]. The NOE build-up curves were obtained from NOESY spectra recorded with mixing times of 100, 150, 200, 250, 300 and 400 ms. Chemical shifts have been referenced to 2,2–dimethyl-2-silapentane-5-sulfonic acid (DSS) as internal standard.

Lipid bilayers were prepared as follows: appropriate quantities of DMPC and F519 were dissolved in chloroform. The solution was evaporated to dryness first by a stream of dry nitrogen and then under vacuum for 3–4 h. A thin film of the lipid and peptide formed on the inner surface of the container which was hydrated with 0.55 ml Tris buffer (pH 7.5). The mixture was allowed to equilibrate for 2 h at 50 °C and then vortexed to give lipid dispersions in aqueous media. The lipid concentration was maintained at 80 mM while the concentration of F519 was varied. Unilamellar vesicles were prepared by sonicating the above dispersions with a sonicator (Branson Sonic Power Co.) at 50% duty cycles until the sample attained optical clarity. In like manner, the control sample (80 mM DMPC) was prepared. ^{31}P NMR experiments were carried out on Varian 600 MHz FT-NMR spectrometer using a broadband probe with proton decoupling (decoupling power 36 dB). The 90° pulse was 10 μs and recycling period was 0.7s.

Molecular Dynamics (MD) Simulations

MD simulations were done on a Silicon Graphics O2 machine with molecular modelling software *Insight II* and *Discover* from Accelrys, USA. Three simulations S1, S2 and S3 for P254 were carried out; each using NMR data in DMSO-d_6, water and HFA, respectively, while simulation S4 was done using NMR data of F519 in DMSO-d_6. The NOEs and coupling constants were used as restraints (*vide infra*) in a simulated annealing protocol (described below) to generate the solution structures.

An extended structure of the peptide was built with the *Biopolymer* module as the starting conformation for the simulations. The energy of the system was calculated with the CFF91 forcefield [20] for P254 while CVFF forcefield [21] was used for F519. The bond stretching in the energy equation was represented by a simple harmonic function. A dielectric constant of 1.0 was used for calculation of electrostatic interactions for simulations S1 and S4, while 4.0 was used for simulations S2 and S3. Before performing an MD run, the starting structure was

thoroughly minimized by a combination of steepest descents and conjugate gradients, to a gradient of 0.01 kcal/mol/Å so as to reduce any internal strain in the starting structure. In the case of simulations S1 and S2 the molecule was slowly 'heated' to 1000 K in steps of 100 K with a 2.5 ps dynamics run. On reaching 1000 K, dynamics was continued for another 25 ps during which period frames at an interval of 1 ps were sampled and stored for further processing. Each of the 25 structures was 'cooled' by gradually lowering the temperature in steps of 100 K to 300 K. For simulations S3 and S4, dynamics was carried out at 300 K. The dynamics was continued after an initialization period of 25 ps for S3 and 50 ps for S4 during which time frames at an interval of 1 ps were sampled and finally subjected to energy minimization. In all four simulations the final minimization with restraints of the annealed structures began with 2000 steps of steepest descents, was followed by 3000 steps of conjugate gradients and terminated with 300 steps of BFGS [22]. At the end of this cycle, most structures had a gradient of 0.01 kcal/mole/Å or lower. In the MD simulations, the Newton's equations of motion were integrated with the Verlet algorithm [23] with a step length of 1 fs. Temperature control was achieved either by scaling the velocities or coupling to a temperature bath.

Distance Restraints

The NOEs were categorized as strong, intermediate and weak with corresponding distance ranges (1.8–2.7 Å), (1.8–3.5 Å) and (1.8–5.0 Å) set for the respective protons. These distances were modified for methyl and methylene groups and for aromatic rings that rotate fast on the NMR time scale. For such groups of protons, it is necessary to define a pseudoatom which is used as a reference point for the distance restraint. Corrections for the distances to such pseudoatoms were made according to the rules initially formulated by Wüthrich [24]. Force constants for distance restraints ranged from 25 to 30 kcal/mol/Å^2. The total number of distance restraints used in the MD simulations is given in Table 1.

Dihedral Restraints

The $^3J_{NH\alpha}$ coupling constant is related to the dihedral angle ϕ as expressed by the relationship [25]:

$$^3J_{NH\alpha} = 6.7\ \cos^2\phi - 1.3\ \cos\phi + 1.5.$$

The coupling constants were transformed to ϕ values which were introduced as dihedral restraints allowing a range of $\pm 10^\circ$ on the calculated values, with a force constant of 25–50 kcal/mol/rad^2. The

Table 1 Summary of Experimental Restraints and Statistical Analysis of the Family of Structures Generated for P254 and F519 by Simulated Annealing

Parameter	P254			F519
Distance restraints	DMSO-d_6	Water	HFA	DMSO-d_6
All	120	109	119	113
Intra-residue	55	43	47	75
Inter-residue	65	66	72	38
Sequential	9	12	14	12
Medium range	54	53	62	26
Long range	2	1	6	—
Dihedral restraints	14	35	25	24
Avg. fractional violation/constraint	0.0038	0.0074	0.0038	0.0106
Avg. no. of violations[a]/structure	1.03	2.08	1.18	3.20
RMSDs with avg. structure: Backbone atoms				
Maximum	0.12	3.72	1.19	3.20
Minimum	0.02	1.18	0.21	1.00
Average	0.04	2.19	0.63	1.86
Average pair-wise RMSD	6.15(±1.4)	3.27(±1.7)	4.42(±2.4)	1.84(±1.3)
IRMA/MARDIGRAS				
R factor	0.53	0.64	0.68	0.58

[a] A ±0.2 Å difference from the imposed distance restraint was considered a violation.

total number of such dihedral restrains used in the MD simulations is listed in Table 1.

Structure Refinement – IRMA (26) and MARDIGRAS (27)

Structure refinement was done using IRMA for S2, S3 and S4 simulations, while structures obtained in S1 simulations were refined by MARDIGRAS. These are computational tools based on NMR relaxation theory. For a given molecular structure, the NOE intensities can be back calculated taking into account the entire spin relaxation network and molecular flexibility. The calculated NOEs are then matched with the experimental values and the structure refined iteratively so that the two closely match. The *R* factor obtained is thus a measure of the fit between the experimental and theoretical NOE intensities.

MARDIGRAS is similar to IRMA, but with the additional capability of using the ROESY spectrum in structure refinement. The IRMA *R* factor is defined as

$$R = \frac{\sum_{\mathrm{i,j,m}} \omega_{\mathrm{ij}}(\tau_{\mathrm{m}})|A_{ij}{}^{\mathrm{cal}}(\tau_{\mathrm{m}}) - A_{\mathrm{ij}}{}^{\mathrm{exp}}(\tau_{\mathrm{m}})|}{\sum_{\mathrm{i,j,m}} \omega_{\mathrm{ij}}(\tau_{\mathrm{m}})|\mathrm{A}_{\mathrm{ij}}{}^{\mathrm{exp}}(\tau_{\mathrm{m}})|}$$

where $A_{ij}{}^{\mathrm{cal}}(\tau_{\mathrm{m}})$ and $A_{\mathrm{ij}}{}^{\mathrm{exp}}(\tau_{\mathrm{m}})$ denote, respectively, the theoretical and experimental NOE intensities for the pair (i,j) for the mixing time τ_{m}. The weight factors ω_{ij} account for measurement errors, particularly noise levels, and were set to 1.0. The *R* factor in MARDIGRAS is given by a similar equation.

The rotational correlation time τ_{c} for P254 was estimated as 2.0 ns from the NOE build-up curve for the CδH of Pro[7] recorded in DMSO and water, and used for the refinement of structures obtained in S1 and S2 simulations. In the case of simulation S3, τ_{c} was calculated as 1 ns from the NOE build-up curve for the CβH of Glu[21] recorded in HFA.

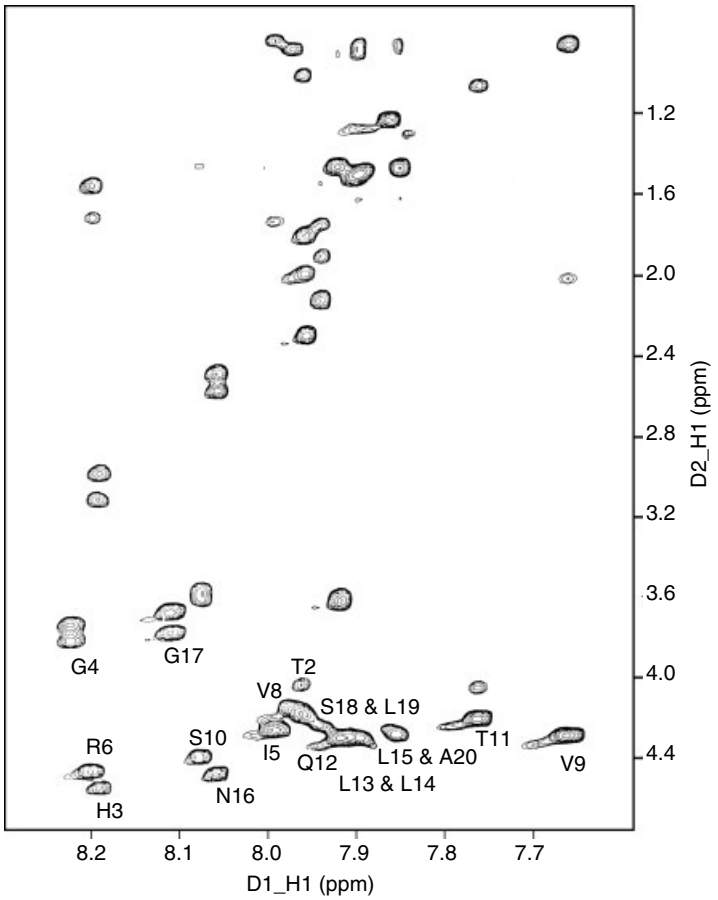

Figure 1 600 MHz TOCSY spectrum of P254 in DMSO-d_6 at 298 K recorded with mixing time of 80 ms (D1 7.6–8.4 ppm and D2 0.8–4.8 ppm).

For the refinement of F519 structures obtained in simulation S4, τ_c was calculated as 4 ns from the NOE build-up curve for the CαH of Gly[16] recorded in DMSO.

RESULTS AND DISCUSSION

The spin systems of the amino acid residues in P254 and F519 that were unique were easily identified in the TOCSY spectra of the respective peptides as seen in Figures 1 and 3. Those that were not unique were grouped together. Thus the unique spin systems such as Thr[2,11], Gly[4,17], Ile[5], Val[8,9], Gln[12,21] and Ala[20] in the case of P254 and Ala[6,14,15,21], Val[2], Gly[3,5,10,13,16,20], Ile[4] and Thr[18] in the case of F519 could be distinguished easily. Ser[10,18], Asn[16] and His[3] of P254 as well as Ser[17,23] and Phe[8,11] of F519, which have the AMX spin-system, were identified as a group of residues. Phe[8,11] in F519 was identified from the NOESY cross peaks arising from its aromatic protons to its α and β protons. Arg[6] in P254 and Arg[22] in F519 was confirmed from peaks from its εNH resonance to its α, β, γ and δ protons. Identification of all leucines in both peptides was done with the help of prominent δ CH_3 NOESY cross peaks. Sequential assignment in all solvents was achieved by the standard procedures using the NOESY spectrum as elaborated in Figures 2 and 4. Once the proton assignment was complete, the ^{13}C assignments were done from the HSQC spectrum by correlating the assigned proton NMR signals to the ^{13}C NMR signals. The ^{13}C assignment helped to confirm all leucine residues in both peptides. The presence of Pro residue at position 7 in P254 caused a break in the assignment. The observation of an NOE between Arg[6] CαH and Pro[7] CδH mended this gap. This NOE also established the '*trans*' state of the Arg[6]–Pro[7] amide bond. In all three media — DMSO-d_6, water (pH 4.5) and HFA — the TOCSY spectra of P254 showed two or more sets of peaks arising from Val[9], Ala[20] and Leu[19] indicating the presence of other minor conformers in equilibrium with the major. In case of F519, Val[2] and Ile[4] exhibited a second set of peaks that could be attributed to a minor conformation.

Table 2 Chemical Shift (ppm), $^3J_{NH\alpha}$ (Hz), and Temperature Coefficients of NH Chemical Shift (ppb/K) of P254 in DMSO-d_6

Residue	NH	CαH	CβH	CγH	Others	$^3J_{NH\alpha}$	Temp coeff.
Cys[1]	—	4.16	2.91, 3.15	—	—	—	—
Thr[2]	7.96	4.19	4.04	1.00	—	8.8	1.6
His[3]	8.20	4.59	2.99, 3.13	—	—	10.9	3.9
Gly[4]	8.22	3.77, 3.84	—	—	—	—	4.0
Ile[5]	7.98	4.27	1.74	1.09, 1.41	δ_1 0.83	8.8	5.7
Arg[6]	8.20	4.49	1.71	1.55	ε NH 7.04, 7.50 δ_1 3.11	8.9	5.2
Pro[7]	—	4.47	2.03	1.86, 1.93	δ_1 3.56, δ_2 3.73	—	—
Val[8]	7.96	4.16	2.00	0.87	—	11.0	3.6
Val[9]	7.66	4.28	2.01	0.86	—	9.6	4.0
Val[9′]	7.63	—	—	—	—	—	—
Ser[10]	8.07	4.41	3.61	—	—	4.8	4.2
Thr[11]	7.76	4.20	4.04	1.05	—	8.9	4.8
Thr[11′]	7.72	—	—	—	—	—	—
Gln[12]	7.94	4.24	1.74, 1.95	2.14	Amide NH 6.79, 7.25	9.3	2.1
Leu[13]	7.88	4.17	1.61	1.48	γ CH_3 0.87	8.9	3.5
Leu[14]	7.09	4.31	—	1.51	γ CH_3 0.86	9.0	3.9
Leu[15]	7.85	4.29	1.61	1.47	γ CH_3 0.86	—	4.0
Asn[16]	8.05	4.50	2.48, 2.56	—	Amide NH 6.99, 7.47	7.9	5.5
Gly[17]	8.11	3.69, 3.80	—	—	—	—	3.4
Ser[18]	7.92	4.31	3.63	—	—	—	3.8
Leu[19]	7.92	4.22	1.77	1.53	γ CH_3 0.89	7.3	3.9
Ala[20]	7.86	4.26	1.22	—	—	8.8	4.2
Glu[21]	7.96	4.21	1.79, 1.99	2.29	—	9.1	4.8

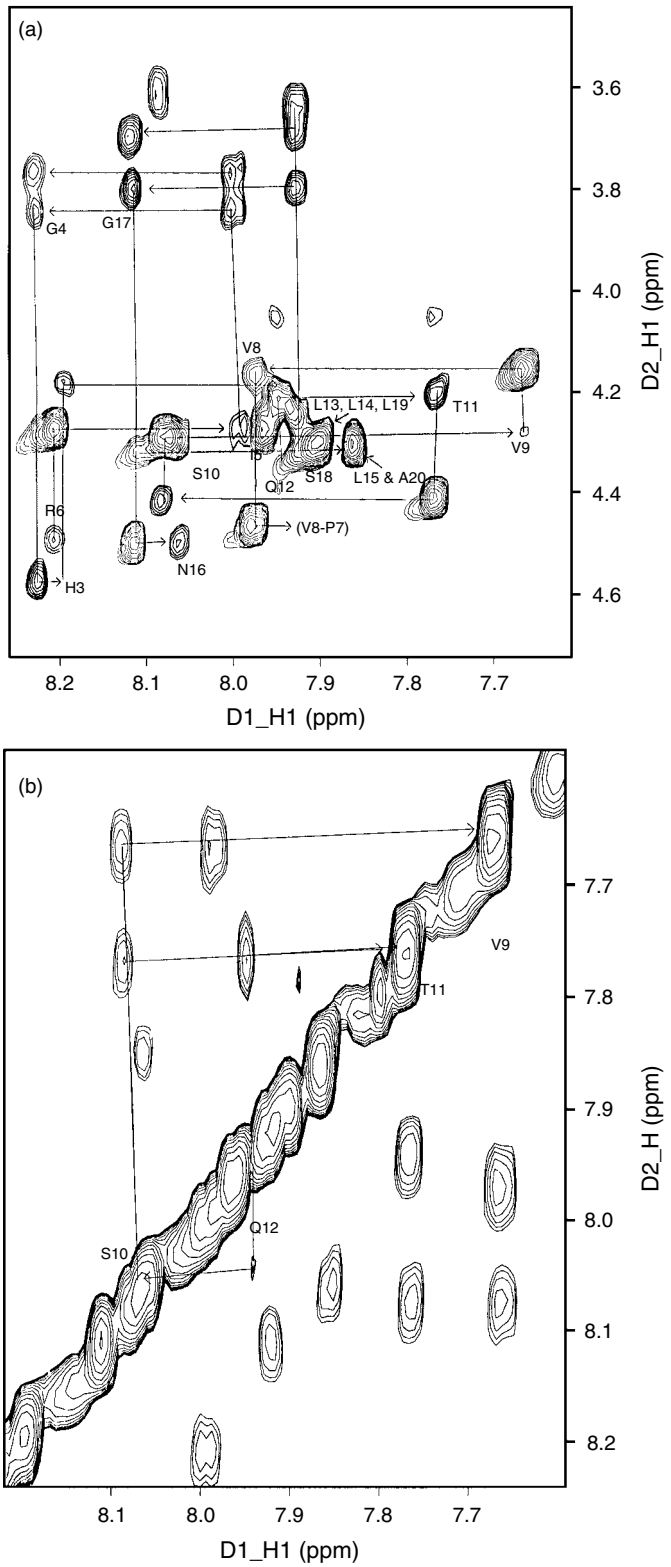

Figure 2 (a) 600 MHz NOESY spectrum of P254 in DMSO-d_6 recorded with mixing time of 300 ms. (D1 7.6–8.4 ppm and D2 3.4–4.8 ppm) (b) NOESY spectrum of P254 in DMSO-d_6 showing the NH-NH region (D1 7.5–8.4 ppm and D2 7.5–8.2 ppm).

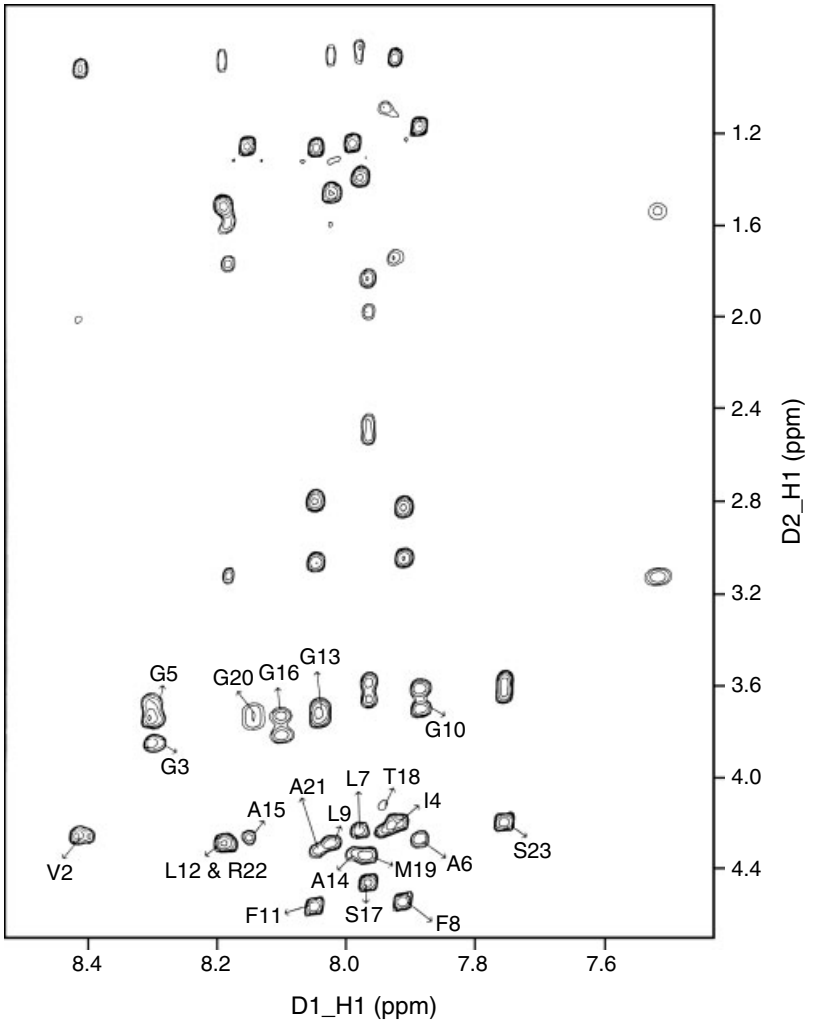

Figure 3 600 MHz TOCSY spectrum of F519 in DMSO-d_6 at 298 K recorded with mixing time of 80 ms. (D1 7.4–8.6 ppm and D2 0.8 to 4.8 ppm).

The minor conformation in both peptides has been estimated at 3%–7% of the major by integration of the relevant cross peaks in the TOCSY spectra. The ^{1}H and ^{13}C chemical shifts for both major and minor conformations of the two peptides are listed in Tables 2–7.

Apart from the NOEs that help in making the assignments, some definite NOE patterns were observed in all solvents which were indicative of specific secondary structures. The NH and αH chemical shift dispersion of P254 in the three solvents were different indicating that its structure differs in the three media. The temperature coefficients of NH chemical shifts provided some clues to possible structures for P254 and F519. The observed temperature coefficient of the NH resonance of Gln^{12} in DMSO-d_6 was 2.1 ppb/K (Table 2) indicating its participation in an intramolecular H-bond while others were beyond the limit of 3.0 ppb/K. Temperature coefficients of NH chemical shifts for all residues in water were above 5 ppb/K (Table 3) showing that all such protons were freely exposed to the solvent. In case of HFA, the temperature coefficient below 5.0 ppb/K of a substantial stretch of residues from Ile^{5} to Gln^{12} (Table 4) suggested intramolecular H-bonds or solvent shielding [11].

The NOESY spectrum of P254 in DMSO-d_6 showed strong NH-NH peaks between Val^{9}-Ser^{10} and between Ser^{10}-Thr^{11} and medium intensity peaks from Ser^{10} αH to Gln^{12} NH (Figure 2b) and Ser^{10} NH to Gln^{12} NH. These NOE peaks

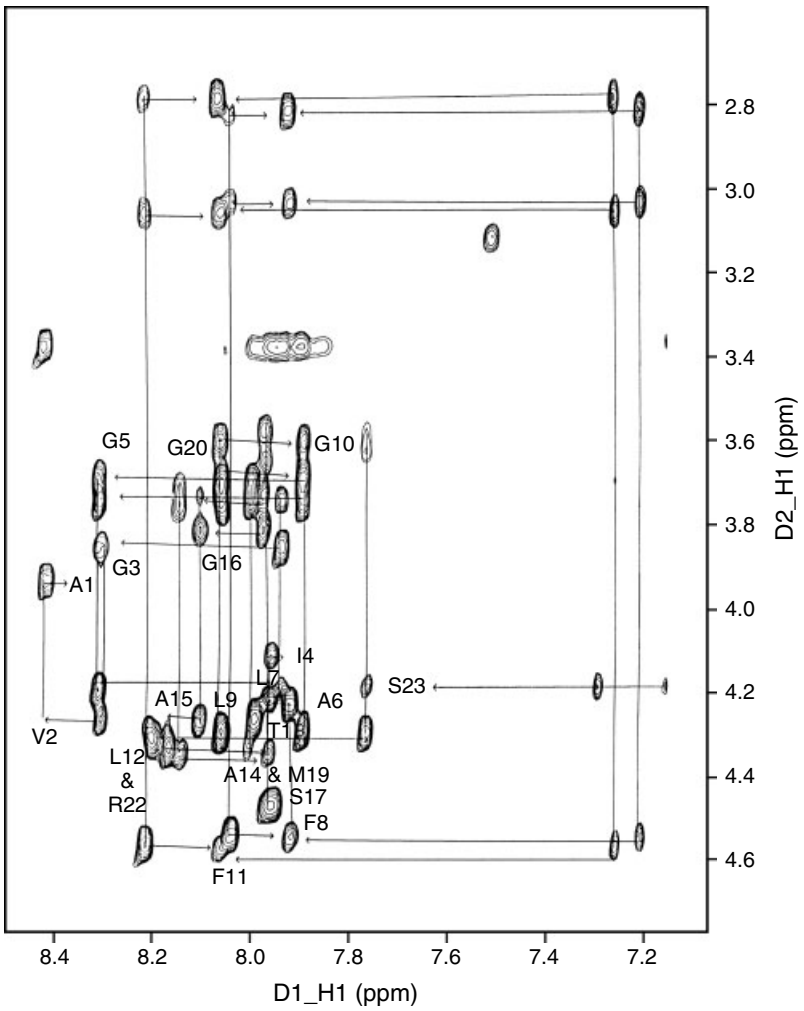

Figure 4 600 MHz NOESY spectrum of F519 in DMSO-d_6 at 298 K recorded with mixing time of 300 ms. (D1 7.4–8.6 ppm, D2 0.8–4.8 ppm).

suggested a Type I β-turn [24] around the tetrad Val^{9}-Ser^{10}-Thr^{11}-Gln^{12}. Support for this comes from the low temperature coefficient of the NH resonance (Table 2) of Gln^{12}. The $^{3}J_{NH\alpha}$ coupling constants for Ser^{10} and Thr^{11} residues deduced from the DQF-COSY spectrum were also strong indicators of a β-turn motif. For the $(i+1)$ residue (Ser^{10}) this value was 4.8 Hz, while 8.9 Hz coupling constant characterized the $(i+2)$ residue (Thr^{11}) in the β-turn. Thus the observed NMR data, namely the pattern of NOEs, low temperature coefficient of the NH chemical shift of Gln^{12} and typical values of $^{3}J_{NH\alpha}$ coupling constants strongly suggested a Type I β-turn around the tetrad Val^{9}–Ser^{10}-Thr^{11}-Gln^{12} for P254 in DMSO. The NMR data for the remaining portion of the peptide best described a random coil.

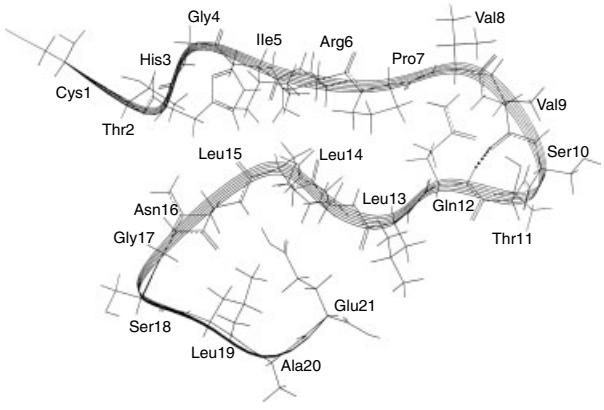

Figure 5 Structure of P254 in DMSO-d_6. The dotted line shows H-bonding in the Type I β-turn. The ribbon traces the backbone atoms.

Table 3 Chemical Shifts (ppm), $^{3}J_{NH\alpha}$ (Hz), and Temperature Coefficients of NH Chemical Shift (ppb/K) of P254 in Water

Residue	NH	CαH	CβH	CγH	Others	$^{3}J_{NH\alpha}$	Temp Coeff.
Cys[1]	—	—	—	—	—	—	—
Thr[2]	8.77	4.29	4.11	1.14	—	7.2	4.5
Thr[2′]	8.75	4.33	—	—	—	—	—
His[3]	8.62	4.73	3.15, 3.29	—	—	7.8	5.2
Gly[4]	8.42	3.94	—	—	—	—	4.1
Ile[5]	8.05	4.17	1.81	1.14, 1.41	δ 0.85	8.6	6.0
Arg[6]	8.35	4.61	1.81	1.69	δ_1 3.16, δ_2 3.29	8.6	6.6
Pro[7]	—	4.42	1.96, 2.25	1.82	δ_1 3.60, δ_2 3.83	—	—
Val[8]	8.22	4.05	2.00	0.91	—	8.5	7.9
Val[9]	8.17	4.16	2.04	0.89	—	9.4	7.5
Ser[10]	8.37	4.48	3.82, 3.88	—	—	7.2	6.5
Thr[11]	8.14	4.25	4.20	1.17	—	—	5.7
Gln[12]	8.26	4.24	1.94, 2.04	2.32	Amide NH 7.25, 6.79	8.4	4.1
Leu[13]	8.08	4.33	1.62	1.54	δ 0.83	8.4	5.2
Leu[14]	7.15	4.32	1.60	—	δ 0.83	8.5	5.7
Leu[15]	8.09	4.28	1.61	1.55	—	7.4	6.6
Asn[16]	8.32	4.64	2.81	—	Amide 7.47, 6.99	8.9	5.3
Gly[17]	8.32	3.93	—	—	—	—	4.5
Ser[18]	8.09	4.43	3.85	—	—	7.3	3.9
Leu[19]	—	—	—	—	—	—	—
Ala[20]	8.14	4.28	1.34	—	—	—	5.0
Glu[21]	8.20	4.39	1.71, 2.18	2.45	—	8.1	6.0

In water, P254 showed sequential NOESY peaks, i.e. peaks between the neighbouring residues that were stronger than the 'COSY' peaks, and medium intensity NH-NH cross peaks. These characteristics provided strong evidence for a β-sheet structure [24]. Further, in this case, the temperature coefficient of NH chemical shifts (Table 3) were above 5 ppb/K indicating that all such protons were freely exposed to the solvent. $^{3}J_{NH\alpha}$ coupling constants of a large number of residues were $\sim$ 8.5 Hz, confirming presence of the β-sheet in water [24]. The $^{13}C\alpha$ chemical shifts all have a negative deviation from the random coil values supporting the β- sheet structure in water [19].

The NOESY spectrum for P254 in the case of HFA, indicated several long range NOE peaks such as Nα(i $\rightarrow$ i + 2, i $\rightarrow$ i + 3) NN (i $\rightarrow$ i + 2) and $\alpha\beta$(i $\rightarrow$ i + 2, i $\rightarrow$ i + 3) stretching from Ile[5] to Gln[12] which were pointers of a helical structure around these residues. Due to a high degree of overlap between NH-α cross peaks of the various residues it was difficult to extract all $^{3}J_{NH\alpha}$ coupling constants from the DQF-COSY spectrum but some values that could be gleaned were near the values characteristic of a helix. Thus in HFA solution, the pattern of long range NOEs, the low temperature coefficients and $^{3}J_{NH\alpha}$ coupling constants suggested a helical structure around Ile[5] to Gln[12] while the remaining part of the peptide adopted a random coil structure.

The NMR data of F519 in DMSO-d_6 showed strong sequential NOESY cross peaks between the neighbouring residues and presence of NH-NH cross peaks which, as previously discussed, are signatures of a β-sheet structure [24]. The temperature coefficients of NH chemical shifts (Table 6), $^{3}J_{NH\alpha}$ coupling constants and $^{13}C\alpha$ CSI values also justify the β-pleated structure [19, 24]. The NMR data thus collectively gave an unequivocal picture of a β-sheet for F519 in DMSO.

A summary of experimental restraints and analysis of the family of structures generated using NMR data for the two peptides by MD simulations is given in Table 1. The simulated structures were refined to *R* factors using IRMA or MARDIGRAS that are also noted in Table 1. The backbone torsion angles (ϕ, φ) averaged over the *ensemble* of

Table 4 Chemical Shift (ppm), $^{3}J_{NH\alpha}$ (Hz), Temperature Coefficients of NH Chemical Shifts (ppb/K) of P254 in HFA

Residue	NH	CαH	CβH	CγH	Others	$^{3}J_{NH\alpha}$	Temp Coeff.
Cys[1]	8.02	4.28	4.02, 3.94	—	—	—	—
Thr[2]	8.29	4.37	4.27	1.20	—	—	—
His[3]	8.37	4.73	3.37, 3.20	—	—	—	—
Gly[4]	8.27	4.05, 3.97	—	—	—	—	—
Ile[5]	7.69	4.31	1.93	1.22, 1.45	δ 0.90, γ 0.95	—	5.6
Arg[6]	8.03	4.48	1.91, 1.75	1.67	δ 3.17	—	—
Pro[7]	—	4.43	2.03, 2.09	1.93	δ_1 3.71, δ_2 3.73	—	—
Val[8]	7.51	3.95	—	—	—	—	6.0
Val[9]	7.78	3.90	—	—	—	—	6.5
Ser[10]	8.00	4.53	3.94	—	—	6.0	4.6
Thr[11]	7.86	4.28	4.00	1.31	—	—	0.9
Gln[12]	8.05	4.03	—	—	—	—	1.7
Leu[13]	8.00	4.14	1.77	1.58	δ 0.92	—	10.2
Leu[14]	7.86	4.21	1.72	1.68	δ 0.92	—	7.9
Leu[15]	8.18	4.21	1.82	1.59	δ 0.90	—	12.5
Asn[16]	8.12	4.66	2.89, 2.95	—	Amide NH 7.47, 6.67	7.3	7.6
Gly[17]	8.20	4.06	—	—	—	—	6.5
Ser[18]	8.07	4.48	3.98	—	—	—	6.8
Leu[19]	7.86	4.42	1.72	1.64	δ 0.91	8.5	6.3
Leu[19′]	7.90	4.46	1.68	1.60	δ 0.90	—	—
Ala[20]	7.79	4.39	1.45	—	—	10.3	4.7
Ala[20′]	8.00	4.41	1.43	—	—	—	—
Glu[21]	7.68	4.23	1.98, 2.15	2.38	—	10.5	5.6

structures for each simulation are given in Tables 8 and 9. Analysis of ϕ, φ angles in simulations S1, S2 and S3 indicated diverse structural representations. In the MD sturtures for P254 in DMSO (S1), ϕ, φ values around the tetrad Val[9]-Ser[10]-Thr[11]-Gln[12] were typical for a Type I β-turn while the remaining portion of the peptide could more appropriately be described as a random coil. In the MD simulation S2, the observed ϕ, φ values indicated a β-sheet. A close inspection of ϕ, φ values of structures obtained from MD simulation S3 for the stretch Ile[5]-Gln[12] confirmed the presence of 3_{10}-helix around this segment, while the rest of the peptide adopted a random coil structure. The analysis of ϕ, φ values of structures in MD simulations S4 indicated the presence of an overall β-sheet for F519. A representation of structures obtained from simulations S1, S2, S3 and S4 is given in Figures 5–8.

F519 was also studied in lipid bilayers to understand the fusogenic properties of this peptide. A convenient method to study lipid polymorphism is through ^{31}P NMR [28]. Since phospholipid molecules contain only one phosphate group, the ^{31}P NMR spectrum is relatively simple. The resonance pattern is governed by the chemical shift anisotropy (CSA) and therefore depends on factors such as the orientation of the applied magnetic field axis, molecular motions of the phosphate group and nature of the lipid organization in the sample. We have carried out ^{31}P NMR experiments on unsonicated as well as sonicated samples of DMPC alone and with a DMPC-F519 mixture (25 : 1). The effect of F519 on DMPC unilamellar vesicles (obtained after sonication of the sample) at different temperatures is shown in Figure 9. In the unsonicated sample of DMPC, which possesses a multilamellar structure, the overall rotational rate is too slow to average the CSA. Thus a powder pattern is observed which consists of a very broad shoulder and a relatively sharp feature. In the sonicated sample of DMPC which is composed largely of unilamellar vesicles, only one sharp peak is observed which

Table 5 ^{13}C Chemical Shift (ppm) of P254 in Different Solvents

Solvent	Residue	α	β	Others
DMSO	Cys[1]	54.40	38.17, 38.21	—
Water		—	33.16	—
DMSO	Thr[2]	61.31	69.54	—
Water		59.10	66.3	γ 18.25
DMSO	His[3]	55.41	43.91	—
Water		—	25.83, 25.85	—
DMSO	Gly[4]	45.47	—	—
Water		42.25	—	—
DMSO	Ile[5]	59.91	40.18	$\gamma_1$27.60, $\gamma_2$27.68, δ 14.47
Water		—	35.47	δ 9.47
DMSO	Arg[6]	55.23	31.56	γ 27.89, δ 49.12
Water		50.48	28.81	γ 26.8, δ 39.9
DMSO	Pro[7]	62.40	31.24	γ 29.70, δ_1 50.20, δ_2 50.21
Water		59.56	28.80	γ 26.80, δ 47.37
DMSO	Val[8]	69.24	32.43	—
Water		59.10	29.58	γ 17.39
DMSO	Val[9]	60.53	32.43	
Water		57.63	29.51	γ 21.51
DMSO	Ser[10]	58.24	64.96	—
Water		54.91	60.58	—
DMSO	Thr[11]	61.31	69.63	—
Water		59.57	66.09	γ 18.32
DMSO	Gln[12]	55.80	34.89	—
Water		58.95	26.01, 26.02	γ 30.44
DMSO	Leu[13]	—	—	γ 27.45, δ 22.67
Water		51.75	—	γ 21.24, δ 20.58
DMSO	Leu[14]	—	—	γ 27.45, δ 21.15
Water		51.72	—	γ 21.33, δ 20.58
DMSO	Leu[15]	54.32	43.86	γ 27.60, δ 21.29
Water		52.00	—	γ 21.14, δ 20.58
DMSO	Asn[16]	52.45	40.34, 40.35	—
Water		50.02	35.40, 35.41	—
DMSO	Gly[17]	45.63	—	—
Water		41.78	—	—
DMSO	Ser[18]	58.68	64.96	—
Water		55.14	60.58	—
DMSO	Leu[19]	54.47	—	γ 26.51
Water		51.72	—	γ 21.33, δ 20.58
DMSO	Ala[20]	51.36	—	—
Water		49.00	15.83	—
DMSO	Glu[21]	54.48	29.77, 33.89	γ 33.36
Water		51.34	25.23, 25.24	—

shifts slightly with increase in temperature. The increase in temperature also brings additional motional averaging and a consequent decrease in linewidth (Figure 9). The effect of F519 on both the multilamellar and unilamellar vesicles of DMPC is remarkable. For the multilamellar case, addition of F519 was seen to increase the CSA *via* an additional line broadening effect. This may be interpreted as an increase in the overall rotational correlation time of the vesicles by F519 (data not shown). In the unilamellar situation, there is a significant alteration of the lipid organization in the presence of F519. The isotropic signal observed for pure DMPC unilamellar vesicles (Figure 9a) changes to

Table 6 Chemical Shift (ppm), $^3J_{NH\alpha}$ (Hz) and Temperature Coefficients of NH Chemical Shift (ppb/K) Coupling Constants of F519 in DMSO-d_6

Residue	NH	CαH	CβH	CγH	Others	$^3J_{NH\alpha}$	Temp Coeff.
Ala[1]	—	3.93	1.33	—	—	—	—
Val[2]	8.41	4.27	2.00	0.90	—	8.4	5.5
Val[2′]	8.39	4.27	—	0.92	—	—	—
Gly[3]	8.30	3.75, 3.85	—	—	—	—	5.3
Ile[4]	7.93	4.21	1.72	1.11, 1.45	δ 0.83, γ 0.86	—	7.0
Ile[4′]	7.90	4.21	—	1.07, 1.47	δ 0.84	—	—
Gly[5]	8.29	3.74, 3.85	—	—	—	—	4.9
Ala[6]	7.88	4.27	1.15	—	—	8.2	5.3
Leu[7]	7.98	4.24	1.53	1.38	δ 0.82	—	5.7
Phe[8]	7.91	4.55	2.82, 3.04	—	2, 6H 7.21	8.4	5.8
Leu[9]	8.03	4.30	1.58	1.45	δ 0.85	—	7.0
Gly[10]	7.88	3.70, 3.60	—	—	—	—	4.9
Phe[11]	8.05	4.57	2.79, 3.06	—	2, 6H 7.26	8.7	6.2
Leu[12]	8.19	4.30	1.61	1.50	δ 0.87	—	7.4
Gly[13]	8.05	3.60, 3.72	—	—	—	—	6.7
Ala[14]	7.99	4.33	1.24	—	—	—	6.0
Ala[15]	8.15	4.27	1.25	—	—	8.3	6.7
Gly[16]	8.09	3.73, 3.81	—	—	—	—	4.9
Ser[17]	7.96	4.47	3.57, 3.66	—	OH 5.19	7.5	4.9
Thr[18]	7.94	4.23	4.11	1.08	OH 4.99	—	6.7
Met[19]	7.96	4.35	1.81, 1.96	2.51	—	—	4.1
Gly[20]	8.13	3.76	—	—	—	—	4.9
Ala[21]	8.05	4.28	1.25	—	—	—	6.0
Arg[22]	8.18	4.30	1.55, 1.75	1.52	δ 3.11, ε 7.50	—	6.3
Ser[23]	7.75	4.19	3.61	—	OH 4.95	9.3	5.2

an anisotropic CSA line shape very much like the multilamellar pattern (Figure 9b). This effect was unaffected by raising the temperature. Thus F519 causes a complete collapse of the isotropic signal to large agglomerates resembling the multilamellar state. The fusogenic properties ascribed to F519 may stem from this behaviour. A similar behaviour has been observed for another peptide very related to F519 [29].

CONCLUSIONS

A hypothetical model for the entire HIV-1 gp120 protein spanning residues 1–510 has been proposed [30]. The model was based on alignment of regions that were conserved within the virus family and present discontinuously throughout the protein but that have similarities in biological, immunological, or genetic properties as predicted by computer algorithms. Our NMR results for P254 show that the stretch of residues from Ile[5] to Gln[12] (258–265) can adopt a 3_{10} helical structure in HFA. A α-helix spanning Ser[18] to Ala[29] (271–282) has been suggested. In the case of DMSO-d_6, a β-turn was observed around the segment Val[9] to Gln[12], which could have some influence in directing the process of protein folding to the native conformation. This turn may constitute the initiation site for the formation of the helix. In water at pH 4.5, the peptide was seen to adopt a β-sheet. It is a known fact that in aqueous environment, the structures of peptides are more flexible and difficult to stabilize as water competes to form hydrogen bonds with the peptide backbone while solvents such as HFA, which provide a hydrophobic surrounding, facilitate the formation of stable secondary structures [31]. The fragment F519, also known as 'fusion peptide', has been studied in lipid membranes to understand

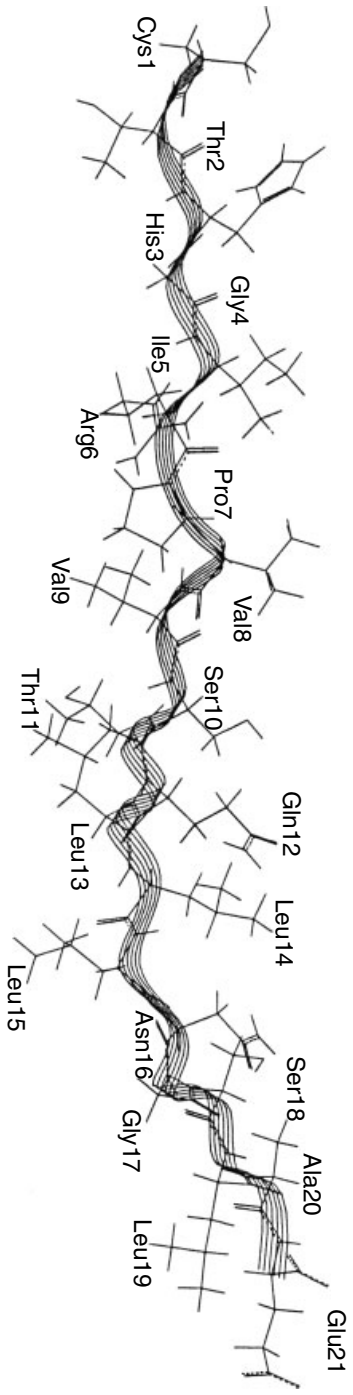

Figure 6 β-Sheet structure of P254 in water. The ribbon traces the backbone atoms.

better the mechanism behind the fusion process [32, 33]. Several reports suggested that the fusion peptide can adopt either a α-helical or β sheet depending on the composition of the lipid membrane and concentration of the peptide with respect to the lipid membrane [32, 33]. When studied with neutral vesicles or erythrocyte ghosts at different peptide : lipid ratios, it was found that the peptide conformation changed from helical to β structure as the peptide: lipid mole ratio was increased from 1 : 200 to 1 : 30 [32, 34]. Chang and co-workers [11] have studied F519 in water, 50% TFE and SDS micellar solution and shown that in aqueous solution it adopted a Type I β-turn around Phe^{8}-Phe^{11}. In 50% TFE, a α helix had been observed for residues spanning Ile^{4}-Ala^{15} with greater stability around the Phe^{8}-Phe^{11} region. Similarly, in SDS micellar solution, a helix had been observed for the region covering residues Val^{2}-Gly^{16}. In the same report, no conclusive answer could be obtained in DMSO but there was a hint of a β-turn structure. Our NMR results show that it unequivocally adopts a β-sheet structure in DMSO. The residues in this fragment are predominantly hydrophobic and postulated to help in insertion into the membrane. Our NMR results for F519 are in line with reports [35, 36] that indicate that F519 is inserted into the membrane presumably as a β-sheet facilitating fusion with the membrane.

Table 7 ^{13}C Chemical Shift (ppm) of F519 in DMSO-d_6

Residue	α	β	Others
Ala^{1}	49.71	19.10	—
Val^{2}	59.25	32.40	γ_1 19.64, γ_2 20.73
Gly^{3}	43.41	—	—
Ile^{4}	58.48	38.21	—
Gly^{5}	43.49	—	—
Ala^{6}	49.71	19.80	—
Leu^{7}	52.66	42.33	γ 25.62, δ 23.19
Phe^{8}	54.91	38.67, 38.68	—
Leu^{9}	52.68	42.41	γ 25.85, δ 23.14
Gly^{10}	43.34	—	—
Phe^{11}	55.30	30.07, 39.06	—
Leu^{12}	52.68	42.25	δ 25.63
Gly^{13}	43.41	—	—
Ala^{14}	49.63	19.64	—
Ala^{15}	—	—	—
Gly^{16}	43.49	—	—
Ser^{17}	56.23	63.15	—
Thr^{18}	59.96	67.65	γ 21.39
Met^{19}	53.67	33.08, 33.08	30.99
Gly^{20}	43.49	—	—
Ala^{21}	49.78	19.64	—
Arg^{22}	53.81	30.36	γ 26.47, δ 41.97
Ser^{23}	56.46	63.22	—

Table 8 Backbone Torsion Angles[a] (ϕ, φ) for HIV-1 P254 in the Three Different Solvents Averaged over Entire Trajectory

Residue	DMSO-d_6		Water		HFA	
	ϕ	φ	ϕ	φ	ϕ	φ
Cys[1]	—	−55 (16) 142 (13)	—	132 (0.7)	—	142 (6)
Thr[2]	−159 (6)	163 (13) −61 (7)	−96 (5)	129 (7)	−79 (5) −137 (12)	118 (15) 154 (8)
His[3]	−160 (8)	169 (10) −79 (14)	−111 (8)	118 (9)	−103 (17) −156 (10)	99 (22) 157 (10)
Gly[4]	−111 (13) 160 (13)	75 (22) −59 (21)	−102 (6) −166 (8)	116 (10)	−134 (20) 163 (16)	−166 (12) 164 (9)
Ile[5]	−154 (6)	152 (8) 97 (24)	−107 (0)	102	−94 (23)	−50 (15)
Arg[6]	−155 (7)	106 (11) 157 (11)	−98 (8)	128 (9)	−61 (3)	−35 (5)
Pro[7]	−80 (17)	172 (6) −172 (2)	−70 (4)	165 (3)	−65 (1)	−37 (3)
Val[8]	−147 (3)	72 (10)	−94 (2)	132 (3)	−66 (2)	−38 (2)
Val[9]	−152 (3)	136 (2)	−94 (1)	135 (1)	−65 (1)	−35 (5)
Ser[10]	−57 (0)	−29 (1)	−121 (0)	104 (0)	−62 (4)	−23 (10)
Thr[11]	−88 (1)	−3 (1)	−131 (2)	104 (1)	−53 (8)	−41 (3)
Gln[12]	−119 (2)	129 (2)	−112 (8)	113 (6)	−165 (4)	121 (7)
Leu[13]	−140 (2)	77 (5)	−110 (6)	116 (9)	−86 (14) −161 (8)	−64 (15)
Leu[14]	−152 (4)	121 (26)	−133 (9)	163 (1)	−152 (6)	−66 (8)
Leu[15]	−157 (6)	−64 (9)	−104 (1)	85 (3)	−159 (5)	151 (10) 85 (10)
Asn[16]	−159 (5)	156 (16) 91 (27)	−166 (2)	127 (8)	−145 (6)	157 (9) 85 (9)
Gly[17]	−120 (19) 115 (7)	−76 (3) 60 (7)	−99 (5) −175 (2)	122 (7)	−141 (3)	113 (1)
Ser[18]	−97 (17) −163 (8)	161 (12) −174 (6)	−102 (7)	−123 (10)	−165 (1)	110 (1)
Leu[19]	−154 (6)	158 (9) 95 (24)	−119 (9)	122 (10)	−128 (1)	111 (1)
Ala[20]	−109 (13) −156 (7)	118 (13) 70 (2)	−117 (8)	108 (3)	−132 (10)	132 (10)
Glu[21]	−73 (13) −134 (16)	—	−95 (2)	—	−158 (14)	—

[a] Torsion angles are in degrees. In parenthesis is the RMSD.

The ^{31}P NMR in DMPC lipid membrane showed how F519 causes fusion of unilamellar vesicles to larger agglomerates like multilamellar ones, giving credence to its name as a 'fusion peptide'. The conformation of P254 is thus seen to be strongly dependent on the environment and points to flexibility being relevant to its biological function. The conformation in a membrane environment may be more relevant than its structure in aqueous or other media.

Acknowledgement

Computational facilities at BCP were provided by the All India Council of Technical Education (AICTE)

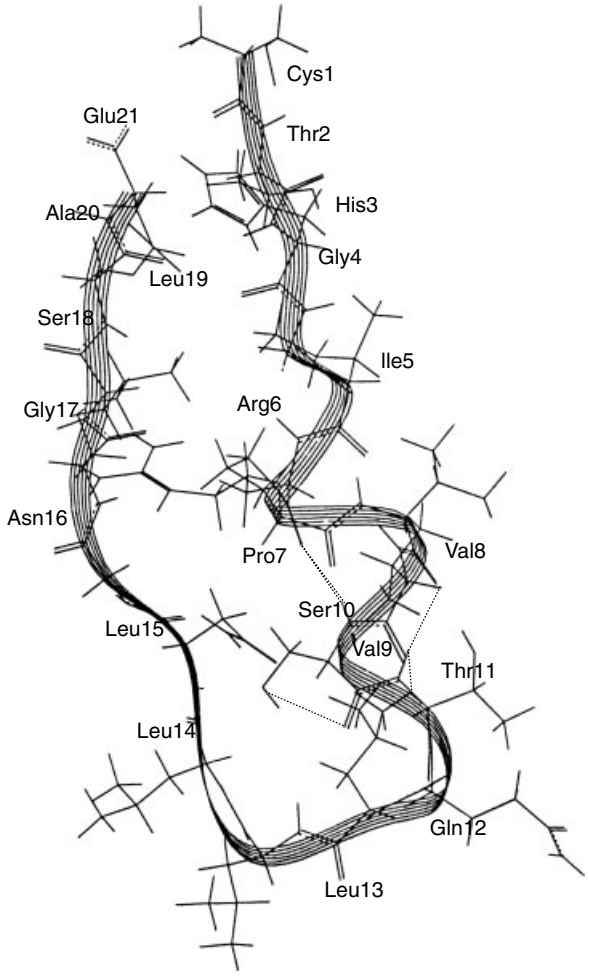

Figure 7 Structure of P254 in HFA. The dotted lines show H-bonding in the 3_{10}-helix. The ribbon traces the backbone atoms.

through Grant F.No. 8017/RDII/MOD/DEG(38)/98-99. The facilities provided by the National Facility for High Field NMR located at TIFR and supported by the Department of Science and Technology (DST) are gratefully acknowledged. Anil Saran thanks the Council of Scientific and Industrial Research (CSIR), New Delhi for support under Emeritus Scientist's scheme. M. Kanyalkar thanks the CSIR, New Delhi for Senior Research Fellowship.

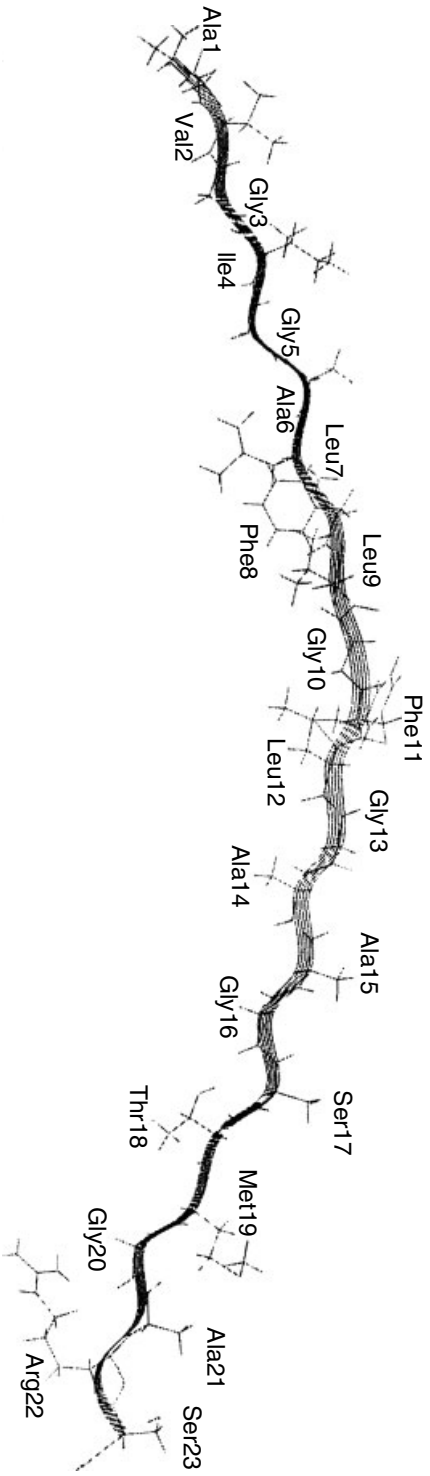

Figure 8 β-Sheet structure of F519 in DMSO-d_6. The ribbon traces the backbone atoms.

REFERENCES

1. Barre-Sinoussi F, Cherman JC, Rey R, Nugeryre MT, Chamaret S, Gruest J, Dauguet C, Axler-Blin C, Rouzioux C, Rosenbaum W, Montagnier L. Isolation of a T-lymphocytropic retrovirus from a patient at risk for acquired immune deficiency syndrome (AIDS). *Science* 1983; **220**: 868–871.

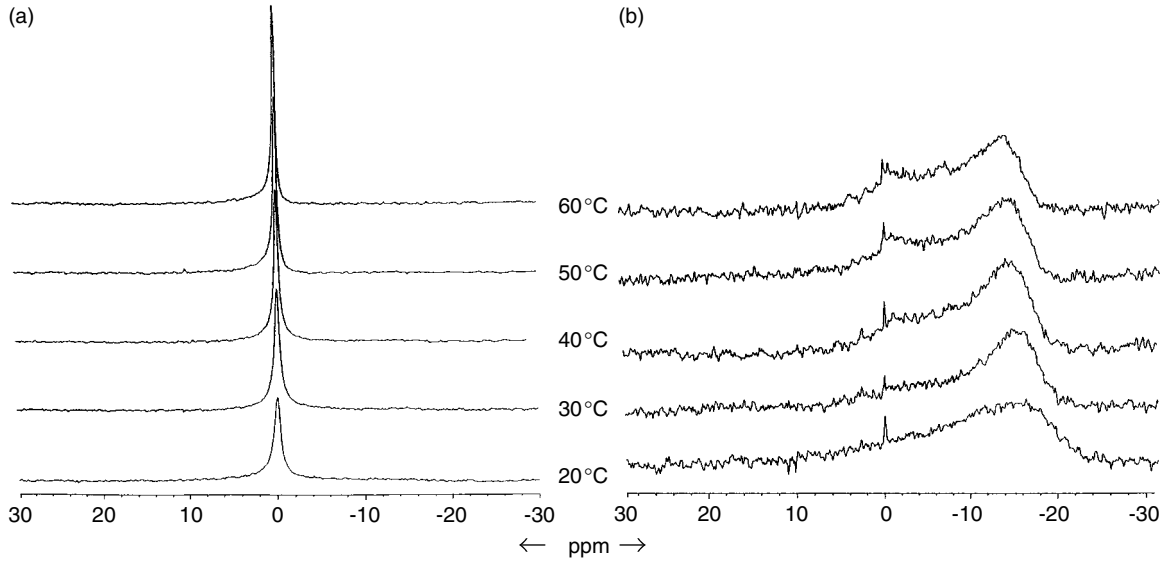

Figure 9 (a)^{31}P NMR spectra of unilamellar DMPC vesicles at different temperatures (number of scans 1024 and line broadening 20 Hz) (b) effect of F519 on unilamellar DMPC vesicles with varying temperatures [identical parameters as (a)].

Table 9 Backbone Torsion Angles[a] (ϕ, φ) for F519 in DMSO Averaged over Entire Trajectory

Residue	DMSO-d_6	
	ϕ	φ
Ala[1]	—	105 (0)
Val[2]	−129 (0)	135 (0)
Gly[3]	−122 (10)	102 (1)
Ile[4]	−119 (13)	124 (4)
Gly[5]	−132 (0)	103 (0)
Ala[6]	−101 (0)	109 (0)
Leu[7]	−99 (0)	129 (0)
Phe[8]	−103 (0)	118 (9)
Leu[9]	−102 (0)	103 (0)
Gly[10]	−114 (9)	137 (1)
Phe[11]	−106 (1)	110 (9)
Leu[12]	−109 (0)	109 (0)
Gly[13]	−108 (0)	107 (0)
Ala[14]	−108 (0)	109 (0)
Ala[15]	−104 (0)	109 (0)
Gly[16]	−108 (0)	107 (0)
Ser[17]	−98 (0)	107 (0)
Thr[18]	−127 (9)	137 (0)
Met[19]	−138 (0)	126 (1)
Gly[20]	−108 (0)	107 (0)
Ala[21]	−102 (1)	130 (4)
Arg[22]	−123 (8)	102 (1)
Ser[23]	−108 (0)	—

[a] Torsion angles are in degrees. In parenthesis is the RMSD

2. Scheid A, Choppin PW. Identification of biological activities of paramyxovirus glycoproteins. Activation of cell fusion, hemolysis, and infectivity by proteolytic cleavage of an inactive precursor protein by Sendai virus. *Virology* 1974; **57**: 475–490.
3. McDougal JS, Mawle AC, Cort SP, Nicholson JKA, Cross DG, Scheppler-Campbell JA, Hicks D, Sligh J. Cellular tropism of the human retrovirus HTLV-III/LAV. Role of T-cell activation and expression of the T4 antigen. *J. Immunol.* 1985; **135**: 3151–3162.
4. McDougal JS, Kennedy SM, Sligh J, Cort SP, Mawle AC, Nicholson JKA. Binding of HTLV-III/LAV to T4$^+$ cells by a complex of the 110K viral protein and the T4 molecule. *Science* 1986; **231**: 382–385.
5. McDougal JS, Nicholson JKA, Cross DG, Cort SP, Kennedy SM, Mawle AC. Binding of the human retrovirus HTLV-III/LAV/ARV/HIV to the CD4 (T4) molecule: Conformation dependence, epitope mapping, antibody inhibition, and potential for idiotypic mimicry. *J. Immunol.* 1986; **137**: 2937–2944.
6. Ho DD, Kaplan JC, Rackauskas IE, Gurney ME. Second conserved domain of Gp120 is important for HIV infectivity and antibody neutralization. *Science* 1988; **239**: 1021–1023.
7. Webster RG, Rott R. Influenza virus A pathogenicity: the pivotal role of hemagglutinin. *Cell* 1987; **50**: 665–666.
8. Kowalski M, Poltz J, Basiripour L, Dorfman T, Goh WC, Terwilliger E, Dayton A, Rosen C, Haseltine W, Sodroski J. Functional regions of the envelope glycoprotein of human immunodeficiency virus type-1. *Science* 1987; **237**: 1351–1355.

9. Lasky la, Nakamura G, Smith JH, Fenie C, Shimosaki L, Patzer E, Berman P, Gregory T, Capon DJ. Delineation of a region of the human immunodeficiency virus type 1 gp120 glycoprotein critical for interaction with the CD4 receptor. *Cell* 1987; **50**: 975–985.
10. Choppin PW, Scheid A. The role of viral glycoproteins in adsorption, penetration, and pathogenicity of viruses. *Rev. Infect. Dis.* 1980; **2**: 40–61.
11. Chang DK, Chien WJ, Cheng AF. The FLG motif in the *N*-terminal region of glycoprotein 41 of human immunodeficiency virus type 1 adopts a type-I β turn in aqueous solution and serves as the initiation site for helix formation. *Eur. J. Biochem.* 1997; **247**: 896–905.
12. Piantini U, Sørensen OW, Ernst RR. Multiple quantum filters for elucidating NMR coupling networks. *J. Am. Chem. Soc.* 1982; **104**: 6800–6801.
13. Bax AD, Davis DG. MLEV-17-based two-dimensional homonuclear magnetization transfer spectroscopy. *J. Magn. Reson.* 1985; **65**: 355–360.
14. Macura S, Huang Y, Suter D, Ernst RR. Two-dimensional chemical exchange and cross-relaxation spectroscopy of coupled nuclear spins. *J. Magn. Reson.* 1981; **43**: 259–281.
15. Dhallium C, Wieruszeski JM, Lippens G. An improved homonuclear TOCSY experiment with minimal water saturation. *J. Magn. Reson. Series B* 1996; **111**: 168–170.
16. Lippens G, Dhallium C, Wieruszeski JM. Use of water flip-back pulse in the homonuclear NOESY experiment. *J. Biomol. NMR* 1995; **5**: 327–333.
17. Khandelwal P, Seth S, Hosur RV. CD and NMR investigations on trifluoroethanol-induced step-wise folding of helical segment from scorpion neurotoxin. *Eur. J. Biochem.* 1999; **264**: 468–478.
18. Kay LE, Keifer P, Sarrinen T. Pure absorption gradient enhanced heteronuclear single quantum correlation spectroscopy with improved sensitivity. *J. Am. Chem. Soc.* 1992; **114**: 10 663–10 665.
19. Wishart DS, Sykes BD, Richards FM. The chemical shift index: A fast and simple method for the assignment of protein secondary structure through NMR spectroscopy. *Biochemistry* 1992; **31**: 1647–1651.
20. Maple J, Dinur U, Hagler AT. Derivation of force field for molecular mechanics and dynamics from ab-initio energy surfaces. *Proc. Natl Acad. Sci. USA* 1988; **85**: 5350–5354.
21. Dauber-Osguthorpe P, Roberts VA, Osguthorpe DJ, Wolff J, Genest M, Hagler AT. Structure and energetics of ligand binding to proteins: *E. coli* dihydrofolate reductase-trimethoprim, a drug-receptor system. *Proteins: Str. Fun. Gen.* 1988; **4**: 31–47.
22. Schlegel HB. Optimisation of equilibrium geometries and transition structures. *J. Comput. Chem.* 1982; **3**: 214–218.
23. Verlet L. Computer experiments on classical fluids. I. Thermodynamical properties of Lennard-Jones molecules. *Phys. Rev.* 1967; **159**: 98–103.
24. Wüthrich K. *NMR of proteins and nucleic acids*. John Wiley & Sons: New York, 1986.
25. Pardi A, Billeter M, Wuthrich K. Calibration of the angular dependence of the amide proton-C_α proton coupling constants, $^3J_{HN\alpha}$, in a globular protein. *J. Mol. Biol.* 1984; **180**: 741–751.
26. Boelens R, Koning TMG, Kaptein R. Determination of biomolecular structure from proton-proton NOE's using a relaxation matrix approach. *J. Mol. Str.* 1988; **173**: 299–311.
27. Borgias BA, James TL. Mardigras — A procedure for matrix analysis of relaxation for discerning geometry of an aqueous structure. *J. Magn. Reson.* 1990; **87**: 475–487.
28. Gorenstein DG. *Phosphorus-31 NMR Principles and Applications*. Academic Press: Orlando, FL, 1984.
29. Curtain C, Separovic F, Nielsen K, Craik D, Zhong Y, Kirkpatrick A. The interactions of the *N*-terminal fusogenic peptide of HIV-1 gp41 with neutral phospholipids. *Eur. Biophys. J.* 1999; **28**: 427–436.
30. Gallaher WR, Ball JM, Garry RF, Martin-Amedee AM, Montelaro RC. A general model for the surface glycoproteins of HIV and other retroviruses. *AIDS Res. Hum. Retrovirus* 1995; **11**: 191–202.
31. Rajan R, Awasthi SK, Bhattacharjya S, Balram P. Teflon-coated Peptides — hexafluoroacetone trihydrate as a structure stabilizer for peptides. *Biopolymers* 1997; **42**: 125–128.
32. Gordon LM, Curtain CC, Zhong YC, Kirkpatrick A, Mobley PW, Waring AJ. The amino-terminal peptide of HIV-1 glycoprotein 41 interacts with human erythrocyte membranes: peptide conformation, orientation and aggregation. *Biochim. Biophys. Acta* 1992; **1139**: 257–274.
33. Mobley PW, Waring AJ, Sherman MA, Gordon LM. Membrane interactions of the synthetic *N*-terminal peptide of HIV-1 Gp41 and its structural analogs. *Biochim. Biophys. Acta* 1999; **1418**: 1–18.
34. Martin I, Schaal H, Scheid A, Ruysschaert JM. Lipid membrane fusion induced by the human immunodeficiency virus type-1 Gp41 *N*-terminal extremity is determined by its orientation in the lipid layer. *J. Virol.* 1996; **70**: 298–304.
35. Agirre A, Flach C, Goni MF, Mendelsohn R, Valpuesta JM, Wu F, Nieva JL. Interactions of the HIV-1 fusion peptide with large unilamellar vesicles and monolayers. A cryo-temp and spectroscopic study. *Biochim. Biophys. Acta* 2000; **1467**: 153–164.
36. Yang J, Gabrys CM, Weilky DP. Solid-state nuclear magnetic resonance evidence for an extended β strand conformation of the membrane-bound HIV-1 fusion peptide. *Biochemistry* 2001; **40**: 8126–8137.

